Self-consistent particle simulation of whistler mode triggered emissions

AUTHOR(S):

Hikishima, Mitsuru; Omura, Yoshiharu; Summers, Danny

CITATION:

Hikishima, Mitsuru ...[et al]. Self-consistent particle simulation of whistler mode triggered emissions. Journal of Geophysical Research 2010, 115: A12246.

ISSUE DATE:

2010-12

URL:

http://hdl.handle.net/2433/134605

JOURNAL OF GEOPHYSICAL RESEARCH, VOL. ???, XXXX, DOI:10.1029/,

Self-consistent particle simulation of whistler-mode triggered emissions

Mitsuru Hikishima,[1] Yoshiharu Omura,[1] Danny Summers[1,2,3]

Abstract. Self-consistent electromagnetic particle simulations have been performed to analyze whistler-mode triggered emissions in the magnetosphere. Triggering whistler-mode waves injected at the magnetic equator induce a nonlinear absolute instability that results in rising tone emissions similar to natural whistler-mode chorus emissions. The triggering wave causes a depletion of resonant electrons at the resonance velocity. The phase-organized resonant electrons released by the triggering waves generate coherent waves that undergo nonlinear growth with increasing frequencies. The essential mechanism is the same as that for the generation of chorus emissions. Saturation of the nonlinear wave growth is caused by enhancement of resonant electrons at high pitch angles that have been trapped and guided along the resonance velocity by the triggered emissions. Because of the decreasing resonance velocity resulting from the increasing frequency, trapped electrons are accelerated to higher pitch angles. Saturation of the nonlinear wave growth thereby results in electron acceleration.

1. Introduction

Magnetospheric whistler-mode waves which occur in the VLF range, 3–30 kHz, can take different forms, including chorus, lightning-generated whistlers, and discrete triggered emissions. Triggered emissions can occur naturally [e.g., *Koons*, 1981; *Okada and Iwai*, 1988; *Anderson and Kurth*, 1989] or be man-made [e.g., *Helliwell*, 1965; *Helliwell and Katsufrakis*, 1974]. Whistler-mode waves also occur in the ELF range, ∼100 Hz to several kHz, as hiss. These various interrelated whistler-mode emissions have significant influence on the physics of the magnetosphere. Electron gyroresonant interaction with chorus is regarded as a key mechanism for generating relativistic electrons in the outer radiation zone [*Summers et al.*, 1998; *Meredith et al.*, 2003; *Katoh and Omura*, 2004; *Varotsou et al.*, 2005; *Summers et al.*, 2007]. Chorus and hiss can cause significant pitch-angle scattering of electrons into the loss cone leading to precipitation losses from the inner magnetosphere [*Kennel and Petschek*, 1966; *Lyons et al.*, 1972; *Lorentzen et al.*, 2001; *Thorne et al.*, 2005; *Summers et al.*, 2007, 2008, 2009]. Man-made VLF triggered emissions constitute a valuable probe of the magnetosphere and thereby enable us to test plasma theory and simulation techniques. Understanding VLF magnetospheric waves requires a self-consistent treatment of the nonlinear gyroresonant interaction of electrons with coherent monochromatic whistler-mode waves. Despite extensive theoretical and numerical studies, e.g., see the review by *Omura et al.* [1991], outstanding questions still remain regarding nonlinear VLF-wave-electron interactions. Recently, considerable progress has been made in understanding magnetospheric chorus emissions by the development of a nonlinear wave growth theory [*Omura et al.*, 2008, 2009] supported by self-consistent particle simulations [*Omura et al.*, 2008; *Hikishima et al.*, 2009a, 2009b, 2010]. The purpose of the present investigation is to apply the recently developed theory and simulations to the analysis of whistler-mode triggered emissions.

With respect to man-made triggered emissions, the triggering signals of duration 0.05–10 sec are emitted from VLF transmitters located, for instance, at Siple [*Helliwell and Katsufrakis*, 1974; *Helliwell*, 1983] or other Antarctic stations. Such signals typically travel along a magnetic field line, and, in the vicinity of the equator, triggered emissions are generated as a result of the interaction of the triggering wave with energetic electrons [*Inan et al.*, 1977; *Kimura et al.*, 1983; *Bell et al.*, 2000]. The triggered emissions are characteristically recorded on the ground at a nearly geomagnetic conjugate location. Triggered emissions are narrow-band ($\Delta f < 100$ Hz), can be relatively long-lasting ($\Delta t \sim 1$ sec), and have a continuous sweep rate of about 1 kHz/sec. Most typically the emissions have an increasing frequency ('risers'), but the frequency may also decrease ('fallers') or exhibit more complex behavior. An over-view of the basic physics of VLF triggered emissions is provided by *Omura et al.* [1991], together with a review of observational studies. A complete understanding of the generation mechanism of VLF triggered emissions has remained elusive for more than 40 years. It has became increasingly apparent that the triggering mechanism involves nonlinear cyclotron resonance between narrow-band whistler-mode waves and energetic electrons [*Nunn*, 1974; *Omura and Matsumoto*, 1985; *Trakhtengerts et al.*, 2001; *Nunn et al.*, 2005]. In particular, resonant currents formed by nonlinear wave trapping are known to play a fundamental role in the generation of whistler-mode triggered emissions [*Omura and Matsumoto*, 1982; *Nunn et al.*, 1997, 2005]. Models employing a Vlasov hybrid simulation (VHS) code have been reasonably successful in reproducing the rising and falling tones of triggered emissions [*Nunn et al.*, 1997, 2003, 2005, 2009]. However, a number of narrowband assumptions have been built into the VHS code, and, as a result, the code does not allow the full evolution of triggered emissions in space, time and frequency. *Katoh and Omura* [2006] performed a self-consistent particle simulation of triggered emissions. In the light of the recently developed theory by *Omura et al.* [2008, 2009], it can now be stated that the mechanism of the rising tone was not adequately described by *Katoh and Omura* [2006].

[1]Research Institute for Sustainable Humanosphere, Kyoto University, Kyoto, Japan.
[2]Department of Mathematics and Statistics, Memorial University of Newfoundland, St. John's, Newfoundland, Canada.
[3]School of Space Research, Kyung Hee University, Yongin, Korea.

0148-0227/11/$9.00

The latter authors tried to explain the frequency variation in terms of the resonant current parallel to the wave magnetic field. However, *Omura et al.* [2008] demonstrated that the resonant current does not contribute to frequency variation of triggered waves.

In this study, we propose to generate VLF triggered emissions by using a self-consistent particle simulation code, and analyze the results by applying the nonlinear wave growth theory developed by *Omura et al.* [2008, 2009]. Details of the simulation code are briefly described in section 2. In section 3 we show and analyze the results for the triggered emissions. The corresponding results for the electron distributions are shown and discussed in section 4. Finally, in section 5 we summarize our results and state our conclusions.

2. Simulation Model

An electromagnetic full-particle simulation is carried out to study wave-particle interaction related to whistler-mode triggered emissions in the inner magnetosphere. We solve Maxwell's equations and the equations of particle motion in space and time self-consistently to treat interactions between electromagnetic waves and plasma particles. The particle simulation scheme and model are described by *Hikishima et al.* [2009a]. The intensity of the ambient magnetic field in the equatorial region is represented by a parabolic function $B_0 = B_{0eq}(1 + ah^2)$ as function of the distance h along the field line from the equator; B_{0eq} is the value of the background magnetic field at the equator, the parabolic coefficient $a = 4.9 \times 10^{-6}(c^{-1}\,\Omega_{e0})^2$ where c is the speed of light, and Ω_{e0} is the equatorial electron gyrofrequency.

Two species of particles, cold electrons and energetic electrons are assumed in the system. The cold electrons determine a cold plasma dispersion relation. The energetic electrons are constructed as a modified anisotropic Maxwellian distribution with a loss cone. The loss cone distribution function of the energetic electrons in the relativistic momentum space $(u_\parallel, u_\perp)$ is realized by the following formula,

$$f(u_\parallel, u_\perp) = \frac{N_h}{(2\pi)^{3/2}U_{th\parallel}U_{th\perp}^2}\exp\left(-\frac{u_\parallel^2}{2U_{th\parallel}^2}\right) \cdot\frac{1}{1-\beta}\left[\exp\left(-\frac{u_\perp^2}{2U_{th\perp}^2}\right) - \exp\left(-\frac{u_\perp^2}{2\beta U_{th\perp}^2}\right)\right], \quad (1)$$

where N_h is the density of energetic electrons, and $U_{th\parallel}$, $U_{th\perp}$ are parallel and perpendicular components of the thermal momentum, respectively, and β is the depth of the loss cone. The thermal momenta $U_{th\parallel} = 0.24c$ and $U_{th\perp} = 0.31c$ of energetic electrons produce a temperature anisotropy $A(= T_\perp/T_\parallel - 1) = 0.7$, where $T_\parallel$ and $T_\perp$ are parallel and perpendicular temperatures, respectively. The cold electron plasma frequency is assumed to be a constant $\omega_{pe} = 5\,\Omega_{e0}$ along the magnetic field line. We neglect the parallel electric field in the direction of the field line to prevent nonphysical diffusion by enhanced thermal fluctuations due to the limited number of superparticles. To suppress the initial thermal fluctuations in the transverse electromagnetic field, we use 134,217,728 superparticles for the energetic electron species. The simulation parameters are listed in Table 1.

In the dipole-like magnetic field, many particles are reflected at their mirror points during the simulation. We assume a loss-cone angle 5.6° at the equator with $L \sim 4$. We calculate equatorial pitch angles of the electrons at the boundaries assuming adiabatic motion. The spatial extent of the regions is $h = \pm 164\,c\Omega_{e0}^{-1}$, including damping regions $\Delta h = 20\,c\Omega_{e0}^{-1}$ at both boundaries of the system. If particles remain outside the loss cone at the boundaries of the simulation system, we reinject them into the simulation system by reversing the parallel velocity. Electrons falling into the loss cone at the boundaries are removed from the system at each time step.

3. Triggered emission

In Figure 1, a schematic illustration for the generation process of triggered emission is shown. Triggering waves with a constant frequency are radiated from the equator. The triggering waves propagate toward higher latitudes and interact with counter-streaming resonant electrons. The resonant electrons are scattered by the triggering waves. The distribution function $f(v_\parallel)$ of energetic electrons then has depletions around the resonance velocities. Triggered rising tone emissions are newly radiated around the equator. The resonance velocities of the triggered emissions decrease in time (Figure 1, *Hikishima et al.* [2009b]). With respect to the evolution of the velocity distribution function, depletions around the resonance velocities of the triggering waves are formed as stationary structures, while the depletions caused by the triggered emissions are progressively shifted toward smaller parallel velocities.

In the previous particle simulation [*Hikishima et al.*, 2009a], it was shown that natural whistler-mode rising emissions are generated near the magnetic equator. In the present simulation, triggering waves are radiated at the magnetic equator. It is assumed that whistler-mode waves with right-handed polarization propagate along the magnetic field line. To realize a whistler-mode wave in the simulation, we assume a linearly polarized sheet current $J_z = I_{z0}\delta(h)\exp(i\omega t)$ at the equator, where $\delta(h)$ is the Dirac delta function. The current generates a linearly polarized wave field, which is decomposed into right- and left-handed polarized waves. The right-handed polarized whistler-mode waves propagate both northward and southward along the magnetic field line, while left-handed polarized waves attenuate as an evanescent mode. We specify I_{z0} so that the transverse wave magnetic field $B_w = 1.3 \times 10^{-3}\,B_{0eq}$ [*Yagitani et al.*, 1992], where $B_w = (B_y^2 + B_z^2)^{1/2}$, B_y and B_z are the components orthogonal to the local magnetic field line. The triggering monochromatic waves with frequency $\omega = 0.2\,\Omega_{e0}$, which is in the unstable frequency range of the linear growth rate (Figure 2, *Hikishima et al.* [2009a]), are injected continuously in time.

We show the time evolution of the triggered wave field together with the triggering waves in Figure 2. Figure 2a shows the spatial and temporal evolution of the transverse wave magnetic field in the entire simulation space. To understand the resonant interaction, we separate the wave magnetic fields B_y and B_z into northward and southward propagating right-handed circularly polarized waves. In Figure 2b, frequency-time power spectrograms are shown at different positions for separate northward and southward propagating waves. At the equator $h = 0\,c\Omega_{e0}^{-1}$, the triggering whistler-mode waves propagate with constant amplitude and frequency. We can confirm that rising tone emissions are clearly generated by the triggering wave with frequency $\omega = 0.2\,\Omega_{e0}$. The triggering whistler-mode waves propagate toward higher latitudes in both hemispheres, being amplified by interaction with anisotropic resonant electrons. The rising tone emissions do not arise directly from the triggering waves through their propagation. Triggered emissions emerge as follows. A triggering wave propagating southward interacts with electrons moving northward, and the electrons are strongly phase-organized in the transverse wave plane. The electrons are released at the equator and move into the region where there is no triggering wave. The phase-organized electrons form a transverse current that generates a new whistler-mode emission propagating southward around $h = 50\,c\Omega_{e0}^{-1}$ at the same frequency as the triggering

wave. The new wave field undergoes nonlinear wave growth with increasing frequency. Similarly for northward propagating waves, the rising tone emission is formed around $h = -50\, c\Omega_{e0}^{-1}$.

We compare the frequency sweep rate derived from nonlinear wave growth theory by *Omura et al.* [2008, 2009] with those of the rising emissions obtained in the simulation. The frequency sweep rate varies as a function of frequency as well as the amplitude of wave. In the simulation, the frequency sweep rates are nearly $\partial\omega/\partial t = 1.2 \times 10^{-4}\, \Omega_{e0}^2$ for northward and southward propagating triggered rising emissions observed near the equator $h = -5$ and $5\, c\Omega_{e0}^{-1}$. Applying the nonlinear growth theory, with a frequency $\omega = 0.3\, \Omega_{e0}$ and a wave amplitude $B_w = 2 \times 10^{-3}\, B_{0eq}$ of the rising tone element, then the frequency sweep rate becomes $\partial\omega/\partial t = 1.1 \times 10^{-4}\, \Omega_{e0}^2$. The agreement of frequency sweep rate with the theory ensures that the nonlinear wave growth theory is valid for triggered rising emissions as well as for natural rising emissions reproduced by *Hikishima et al.* [2009a] using an electromagnetic particle code.

The resonant electrons that interact with the triggering waves are strongly modified in the velocity phase space. The phase-organized electrons move beyond the injection point at the equator, penetrating into the opposite hemispheres. The left panel of Figure 2a shows that phase-organized electrons interacting with a southward triggering wave can radiate waves in the northern hemisphere with an amplitude comparable to that of the triggering wave. The radiated waves in the northern hemisphere turn into an emission undergoing nonlinear wave growth [*Omura et al.*, 2008, 2009]. The nonlinear wave growth corresponds to an absolute instability with a coherent wave phase. We find that the absolute instability takes place around $h = 50\, c\Omega_{e0}^{-1}$ during the time period $t = 4200$–$6700\, \Omega_{e0}^{-1}$. In the right panels of Figure 2b, we find that the same process takes place for the northward triggering wave, and the absolute instability occurs at $h = -50\, c\Omega_{e0}^{-1}$ over the same time period.

The generation of natural rising emissions from a background of wave noise was demonstrated by *Hikishima et al.* [2009a]. We must show that the appearance of the rising emission in Figure 2 is due to triggering waves and not from naturally rising emissions growing from noise. A simulation run without the injection of a triggering wave is carried out. The other simulation parameters are the same as those for the simulation shown in Figure 2. In Figure 3 the results are shown for the same wave separation and in the same dynamic ranges of wave intensity as in Figure 2. Whistler-mode waves are induced from noise in the whole region, and grow through cyclotron resonant interaction with anisotropic resonant electrons. Weak whistler-mode waves propagate toward both hemispheres, with moderate growth. The frequency structure 0.1–0.3 Ω_{e0} in Figure 3b is almost constant in time. The frequency does not show any frequency variation because the amplitude remains under the threshold level $B_{th} = 2.8 \times 10^{-4}\, B_{0eq}$ (corresponding to $\omega = 0.2\Omega_{e0}$) for nonlinear wave growth [*Omura et al.*, 2009]. The wave development is due only to the positive linear growth rate. Comparison of the results in Figures 2 and 3 demonstrates that the generation of the rising tone emission is due to the injected triggering whistler-mode waves.

4. Electron distribution

Triggered waves as well as the triggering waves in the simulation should scatter resonant electrons nonlinearly [*Hikishima et al.*, 2009b, 2010]. In Figure 4, the time evolution of the velocity distribution function of energetic electrons $f(v_\parallel, v_\perp)$ around the equator is shown. Triggering waves are continuously injected at the equator. A triggered emission appears over the time interval $t = 4000$–$7000\, \Omega_{e0}^{-1}$ at the equator, as shown in Figure 2b. Before the triggered emission appears ($t < 4000\, \Omega_{e0}^{-1}$), triggering waves at the frequency $\omega = 0.2\, \Omega_{e0}$ scatter resonant electrons. The resonance velocities associated with the triggering waves are $V_R \sim \pm 0.3\, c$, which correspond to points on a (relativistic) ellipse in velocity $(v_\parallel, v_\perp)$ space. Significant scattering of resonant electrons over a wide range of energy with different pitch angles is seen near the tail of the distribution function. The scattering results in deformation of the distribution function. The triggering waves drive some of the resonant electrons into the loss cone. At $t > 4000\, \Omega_{e0}^{-1}$, triggered emissions are generated with rising frequencies. With wave frequencies rising in time, the resonance velocities V_R decrease toward smaller parallel velocities, as determined by the cyclotron resonance condition. At a higher frequency $\omega \sim 0.7\, \Omega_{e0}$, the wave intensities of the triggered emissions become weak, thereby scattering fewer resonant electrons. In Figure 4b we plot perspective views of the same distribution function shown in Figure 4a. While we find depletion of electrons at lower pitch angles, we also find enhancement of electrons along the resonance velocity at higher pitch angles.

From $t = 1311\, \Omega_{e0}^{-1}$, scattering and depletion of resonant electrons by the triggering waves with a constant frequency are observed. However, the depletion cannot be observed at larger $v_\perp$, although the intensity of the triggering wave is strong and constant in time. In addition to scattering by the triggering waves, the velocity distribution function after $t = 4014\, \Omega_{e0}^{-1}$ indicates distinct scattering by the triggered emissions. At lower perpendicular velocities, the triggered emissions scatter resonant electrons, resulting in enhanced depletion of the distribution function. However, at higher perpendicular velocities, $v_\perp > 0.5\, c$, the electron density slightly increases and forms bumps along the resonance curves. The bumps on the distribution function move toward smaller parallel velocity with increasing frequency of the triggered emissions.

In Figure 5, we show the time evolution of the distribution function $f(v_\parallel)$ at (a) $v_\perp = 0.3\, c$ and (b) $v_\perp = 0.6\, c$, around the equator. The initial distribution function $f(v_\parallel)$ at $t = 0\, \Omega_{e0}^{-1}$ is superimposed on the figure at each time step as a dashed form for comparison. At $v_\perp = 0.3\, c$, Figure 5a shows that the depletion of the distribution function at $|v_\parallel| \sim 0.3\, c$ by the triggering waves begins at $t = 1311\, \Omega_{e0}^{-1}$. Since the frequency of the triggering waves is constant, depletions of the distribution function do not shift. While undergoing nonlinear pitch-angle scattering, resonant electrons are swept in the direction of larger parallel velocities. The number of untrapped resonant electrons is larger than that of trapped resonant electrons. Trapped electrons are nonlinearly scattered toward smaller parallel velocities, as opposed to the transfer of untrapped electrons toward larger parallel velocities. Slightly visible enhancements of the electron distribution are produced at $t = 1311\, \Omega_{e0}^{-1}$ around velocities greater than the resonance velocities. On the other hand, depletions produced by triggered emissions are shifted progressively toward smaller parallel velocities. The magnitude of the depletions is remarkable compared with those of the triggering waves. Since the amplitude of the triggered waves are shown to increase in time with increasing frequency, the depletion is more pronounced. At $v_\perp = 0.6\, c$, depletions by the triggering waves are not seen in Figure 5b. In contrast to the depletions of the distribution function at lower $v_\perp$, distinct electron bumps appear at the resonance velocities of the triggered emissions, which shift to smaller parallel velocities due to the frequency shift. The resonance velocities of the triggered emissions sweep through the velocity phase space corresponding to the rising frequencies, There then arises a wave potential trough in space that traps resonant electrons at larger parallel velocities at some distance from the equator and guides them to smaller parallel velocities near the equator. Through the trapping process produced

by the triggered rising tone emissions, resonant electrons are effectively accelerated toward higher pitch angles. Entrapping of the resonant electrons is especially effective at the front of the wave packets which grow in amplitude as they propagate away from the equator.

We find in Figure 2a that a triggered rising emission emerges from the equatorial region where no triggering wave exists. The corresponding modification of the velocity distribution function of energetic electrons should contribute to the generation process. The time evolution of the distribution functions $f(v_\parallel, v_\perp, h)$ of energetic electrons at $v_\perp = 0.3c$ and $v_\perp = 0.6c$ are plotted in Figures 6a and 6b, respectively. To show the deviation from the unperturbed distribution function $f_0(v_\parallel, v_\perp, h)$ at $t = 0\ \Omega_{e0}^{-1}$, we plot $(f - f_0)/f_0$. In the distribution function at $v_\perp = 0.3\ c$, electrons with positive $v_\parallel$ interact with the triggering wave propagating southward from the equator, collecting around the resonance velocity indicated by the white dashed line. A depletion develops even in the northern hemisphere ($h > 0$) where there exists no triggering wave. This is because the resonant electrons scattered around the resonance velocity in the southern hemisphere move into the northern hemisphere, undergoing adiabatic motion to maintain the structure in the velocity phase space. The same process takes place for electrons with negative $v_\parallel$ interacting with the triggering wave propagating northward.

In the simulation, electrons outside the loss cone bounce back at the boundaries. Outgoing depletion of electrons from the simulation region appears at the boundaries, with reversed parallel velocities. However, the depletions do not affect the formation of triggered rising waves near the equator. Depletion at lower frequencies of the triggered rising tone emissions begins to appear at $t = 3277\ \Omega_{e0}^{-1}$ at higher latitudes. Higher frequency waves induce depletions at lower parallel velocities. As a result of the rising frequency, the depletions move progressively toward lower parallel velocities. The depletions become larger as the wave amplitudes of the triggered emissions grow.

At the higher perpendicular velocity $v_\perp = 0.6\ c$, corresponding to the bumps of the resonant electrons we find in Figures 4b and 5b, enhancements of the distribution function along the resonance velocities of the rising tone emissions near the equator. This is due to efficient entrapping of resonant electrons at the front of the wave by the trapping potentials of the triggered emissions. The trapped electrons move toward the equator guided along the resonance velocity of the triggered emissions. Because of the rising tones of the two triggered emissions propagating northward and southward, the two bumps approach the line $v_\parallel = 0\ c$ near the equator. The electrons forming the bumps are accelerated to higher energies, and remain trapped magnetically with high pitch angles. It is expected that further triggered rising emissions should cause an accumulation of accelerated electrons. The process would result in a pancake distribution seen in the localized region near the equator, as demonstrated by *Hikishima et al.* [2009b].

To illustrate the spatial evolution of the triggered emissions with varying frequency, we plot the time evolution of frequency-space ($\omega - h$) spectrograms of southward and northward propagating waves in Figures 7a and 7b, respectively. Figure 7 illustrates very well the guiding of resonant electrons that are trapped by the growing potential of the triggered emissions. This feature is demonstrated in Figure 6b ($t = 4997$–$6799\ \Omega_{e0}^{-1}$). Triggering waves with a constant frequency $\omega = 0.2\ \Omega_{e0}$ are radiated from the equator ($h = 0\ c\Omega_{e0}^{-1}$), and propagate into both hemispheres. The triggering waves grow because of the positive linear growth rate as they propagate away from the equator. Generation regions of triggered emissions are found around $|h| \sim 50\, c\Omega_{e0}^{-1}$ at higher frequencies. Triggered emissions begin to appear at a frequency slightly above the frequency of the triggering wave. As the frequency increases, the generation locations of the triggered emissions shift toward higher latitudes ($|h| \sim 70 c\Omega_{e0}^{-1}$). Frequencies of the triggered waves do not change during the cause of their propagation.

5. Summary

1. We have performed a self-consistent particle simulation with triggering whistler-mode waves radiated from the magnetic equator. The amplitude of the triggering wave is greater than the threshold value given by nonlinear wave growth theory [*Omura et al.*, 2009]. Seeds of the rising emissions are generated from the phase-organized electrons that are released from the triggering waves at the equator.

2. The initial phase of the triggered rising emissions shows the nonlinear wave growth as described by the chorus equations (equations of (40) and (41) of *Omura et al.* [2009]). The frequency sweep rate of the triggered emissions agrees with the theoretical estimate deduced from the wave amplitude of the triggering waves.

3. Comparison between the simulation run with triggering waves and a run without triggering waves demonstrates that nonlinear wave growth is different from linear wave growth driven by a temperature anisotropy. The nonlinear growth rates can be much larger than the linear growth rates.

4. Saturation of the nonlinear wave growth of the triggered emissions is due to the formation of bumps at large $v_\perp$ in the velocity phase space in the later phase of the rising tone emissions. The bumps are formed by resonant electrons which are guided toward the equator by the wave packets of the triggered emissions which propagate away from the equator with growing amplitudes. Because of the decreasing resonance velocity due to the increasing frequency, trapped electrons are accelerated to higher pitch angles. Electron acceleration results from the saturation of the nonlinear wave growth process.

Acknowledgments. The computation in this study was performed on the KDK system of RISH at Kyoto University. This work was supported by Grant-in-Aid 20340135 of the Ministry of Education, Science, Sports and Culture of Japan. D.S. acknowledges support from the Natural Sciences and Engineering Research Council of Canada under grant A-0621 and additional support by WCU grant R31-10016 funded by the Korean Ministry of Education, Science and Technology.

References

Anderson, R. R., W. S. Kurth (1989), Discrete electromagnetic emissions in planetary magnetospheres, in *Plasma Waves and Instabilities at Comets and in Magnetospheres*, *Geophys. Monogr. Ser.*, vol. 53, edited by B. T. Tsurutani and H. Oya, p.81, AGU, Washington, D. C.

Bell, T. F., U. S. Inan, R. A. Helliwell, and J. D. Scudder (2000), Simultaneous triggered VLF emissions and energetic electron distributions observed on POLAR with PWI and HYDRA, *Geophys. Res. Lett.*, *27*(2), 165.

Helliwell, R. A. (1965), *Whistlers and Related Ionospheric Phenomena*, Stanford Univ. Press, Stanford, Calif.

Helliwell, R. A. (1983), Controlled stimulation of VLF emissions from Siple Station, Antarctica, *Radio Sci.*, *18*(6), 801.

Helliwell, R. A., and J. P. Katsufrakis (1974), VLF wave injection into the magnetosphere from Siple Station, Antarctica, *J. Geophys. Res.*, *79*(16), 2511.

Hikishima, M., S. Yagitani, Y. Omura, and I. Nagano (2009a), Full particle simulation of whistler-mode rising chorus emissions in the magnetosphere, *J. Geophys. Res.*, *114*, A01203, doi:10.1029/2008JA013625.

Hikishima, M., S. Yagitani, Y. Omura, and I. Nagano (2009b), Coherent nonlinear scattering of energetic electrons in the process of whistler mode chorus generation, *J. Geophys. Res.*, *114*, A10205, doi:10.1029/2009JA014371.

Hikishima, M., Y. Omura, and D. Summers (2010), Microburst precipitation of energetic electrons associated with chorus wave generation, *Geophys. Res. Lett.*, *37*, L07103, doi:10.1029/2010GL042678.

Inan, U. S., T. F. Bell, D. L. Carpenter, and R. R. Anderson (1977), Explorer 45 and Imp 6 observations in the magnetosphere of injected waves from the Siple Station VLF transmitter, *J. Geophys. Res.*, *82*(7), 1177.

Katoh, Y., and Y. Omura (2004), Acceleration of relativistic electrons due to resonant scattering by whistler mode waves generated by temperature anisotropy in the inner magnetosphere, *J. Geophys. Res.*, *109*, A12214, doi:10.1029/2004JA010654.

Katoh, Y. and Y. Omura (2006), A study of generation mechanism of VLF triggered emission by self-consistent particle code, *J. Geophys. Res.*, *111*, A12207, doi:10.1029/2006JA011704.

Kennel, C. F., and H. E. Petschek (1966), Limit on stably trapped particle fluxes, *J. Geophys. Res.*, *71*(1), 1.

Kimura, I., H. Matsumoto, T. Mukai, K. Hashimoto, T. F. Bell, U. S. Inan, R. A. Helliwell, and J. P. Katsufrakis (1983), EXOS-B/Siple Station VLF wave-particle interaction experiments: 1. General description and wave-particle correlations, *J. Geophys. Res.*, *88*(A1), 282.

Koons, H. C. (1981), The role of hiss in magnetospheric chorus emissions, *J. Geophys. Res.*, *86*(A8), 6745.

Lorentzen, K. R., J. B. Blake, U. S. Inan, and J. Bortnik (2001), Observations of relativistic electron microbursts in association with VLF chorus, *J. Geophys. Res.*, *106*(A4), 6017.

Lyons, L. R., R. M. Thorne, and C. F. Kennel (1972), Pitch-angle diffusion of radiation belt electrons within the plasmasphere, *J. Geophys. Res.*, *77*(19), 3455.

Meredith, N. P., M. Cain, R. B. Horne, R. M. Thorne, D. Summers, and R. R. Anderson (2003), Evidence for chorus-driven electron acceleration to relativistic energies from a survey of geomagnetically disturbed periods, *J. Geophys. Res.*, *108*(A6), 1248, doi:10.1029/2002JA009764.

Nunn, D. (1974), A self consistent theory of triggered VLF emissions, *Planet. Space Sci.*, *22*, 349.

Nunn, D., Y. Omura, H. Matsumoto, I. Nagano, and S. Yagitani (1997), The numerical simulation of VLF chorus and discrete emissions observed on the Geotail satellite using a Vlasov code,*J. Geophys. Res.*, *102*(A12), 27,083.

Nunn, D., A. Demekhov, V. Trakhtengerts, and M. J. Rycroft (2003), VLF emission triggering by a highly anisotropic electron plasma, *Ann. Geophys.*, *21*, 481.

Nunn, D., M. Rycroft, and V. Trakhtengerts (2005), A parametric study of the numerical simulations of triggered VLF emissions, *Ann. Geophys.*, *23*, 3655.

Nunn, D., O. Santolik, M. Rycroft, and V. Trakhtengerts (2009), On the numerical modelling of VLF chorus dynamical spectra, *Ann. Geophys.*, *27*, 2341.

Okada, T., and A. Iwai (1988), *Natural VLF radio waves*, Res. Stud. Press, New York.

Omura, Y., and H. Matsumoto (1982), Computer simulations of basic processes of coherent whistler wave-particle interactions in the magnetosphere, *J. Geophys. Res.*, *87*(A6), 4435.

Omura, Y., and H. Matsumoto (1985), Simulation study of frequency variations of VLF triggered emissions in a homogeneous field, *J. Geomagn. Geoelectr.*, *37*, 829.

Omura, Y., D. Nunn, H. Matsumoto, and M. J. Rycroft (1991), A review of observational, theoretical and numerical studies of VLF triggered emissions, *J. Atmos. Terr. Phys.*, *53*, 351.

Omura, Y., Y. Katoh, and D. Summers (2008), Theory and simulation of the generation of whistler-mode chorus, *J. Geophys. Res.*, *113*, A04223, doi:10.1029/2007JA012622.

Omura, Y., M. Hikishima, Y. Katoh, D. Summers, and S. Yagitani (2009), Nonlinear mechanisms of lower-band and upper-band VLF chorus emissions in the magnetosphere, *J. Geophys. Res.*, *114*, A07217, doi:10.1029/2009JA014206.

Summers, D., R. M. Thorne, and F. Xiao (1998), Relativistic theory of wave-particle resonant diffusion with application to electron acceleration in the magnetosphere, *J. Geophys. Res.*, *103*(A9), 20,487.

Summers, D., B. Ni, and N. P. Meredith (2007), Timescales for radiation belt electron acceleration and loss due to resonant wave-particle interactions: 2. Evaluation for VLF chorus, ELF hiss, and electromagnetic ion cyclotron waves, *J. Geophys. Res.*, *112*, A04207, doi:10.1029/2006JA011993.

Summers, D., B. Ni, N. P. Meredith, R. B. Horne, R. M. Thorne, M. B. Moldwin, and R. R. Anderson (2008), Electron scattering by whistler-mode ELF hiss in plasmaspheric plumes, *J. Geophys. Res.*, *113*, A04219, doi:10.1029/2007JA012678.

Summers, D., R. Tang, and R. M. Thorne (2009), Limit on stably trapped particle fluxes in planetary magnetospheres, *J. Geophys. Res.*, *114*, A10210, doi:10.1029/2009JA014428.

Thorne, R. M., T. P. O'Brien, Y. Y. Shprits, D. Summers, and R. B. Horne (2005), Timescale for MeV electron microburst loss during geomagnetic storms, *J. Geophys. Res.*, *110*, A09202, doi:10.1029/2004JA010882.

Trakhtengerts, V. Y., Y. Hobara, A. G. Demekhov, and M. Hayakawa (2001), A role of the second-order cyclotron resonance effect in a self-consistent approach to triggered VLF emissions, *J. Geophys. Res.*, *106*(A3), 3897.

Varotsou, A., D. Boscher, S. Bourdarie, R. B. Horne, S. A. Glauert, and N. P. Meredith (2005), Simulation of the outer radiation belt electrons near geosynchronous orbit including both radial diffusion and resonant interaction with whistler-mode chorus waves, *Geophys. Res. Lett.*, *32*, L19106, doi:10.1029/2005GL023282.

Yagitani, S., I. Nagano, Y. Omura, and H. Matsumoto (1992), Comparison between particle simulation and full-wave analysis for wave propagation in a nonuniform plasma, *Radio Sci.*, *27*(4), 449.

M. Hikishima, Y. Omura, D. Summers, Research Institute for Sustainable Humanosphere, Kyoto University, Uji, Kyoto 611-0011, Japan. (hikishima@rish.kyoto-u.ac.jp; omura@rish.kyoto-u.ac.jp; summers@rish.kyoto-u.ac.jp)

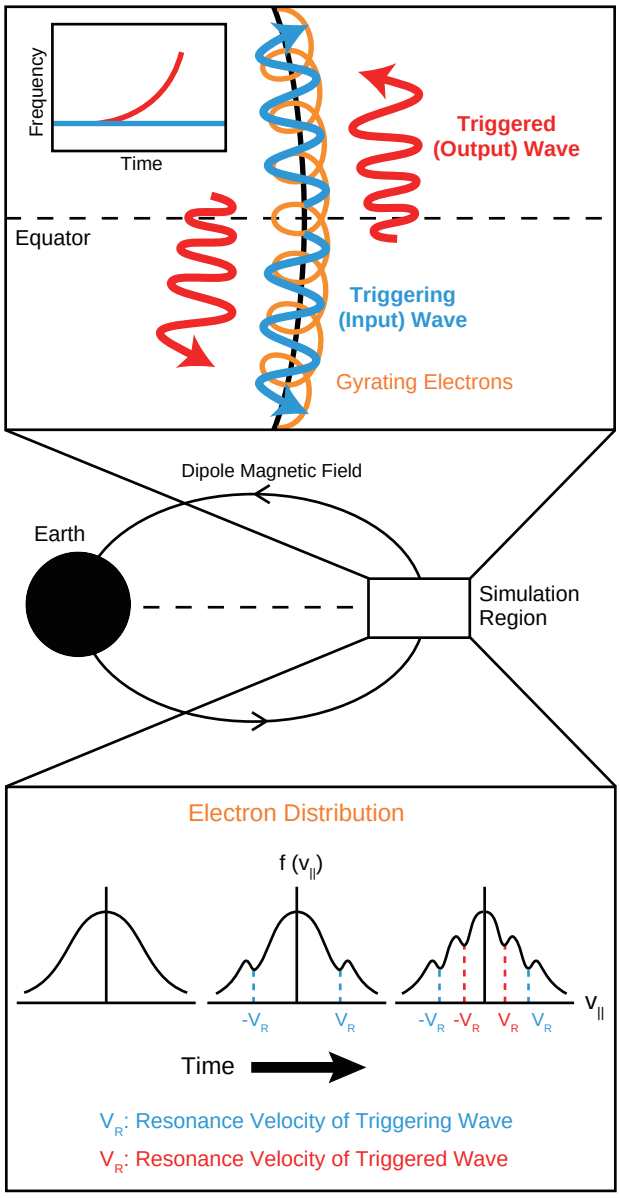

Figure 1. Schematic illustration of propagating triggering and triggered waves, and corresponding electron distribution functions. The triggering waves with constant frequency are injected at the equator and propagate into both hemispheres. The triggering waves resonate with counter-streaming resonant electrons. The electron distribution functions acquire enhanced depletions along the resonance velocities $\pm V_R$ (blue). The unstable distribution functions excite triggered waves which appear with rising frequency. The triggered rising waves cause depletions at the resonance velocities $\pm V_R$ (red) in the distribution function.

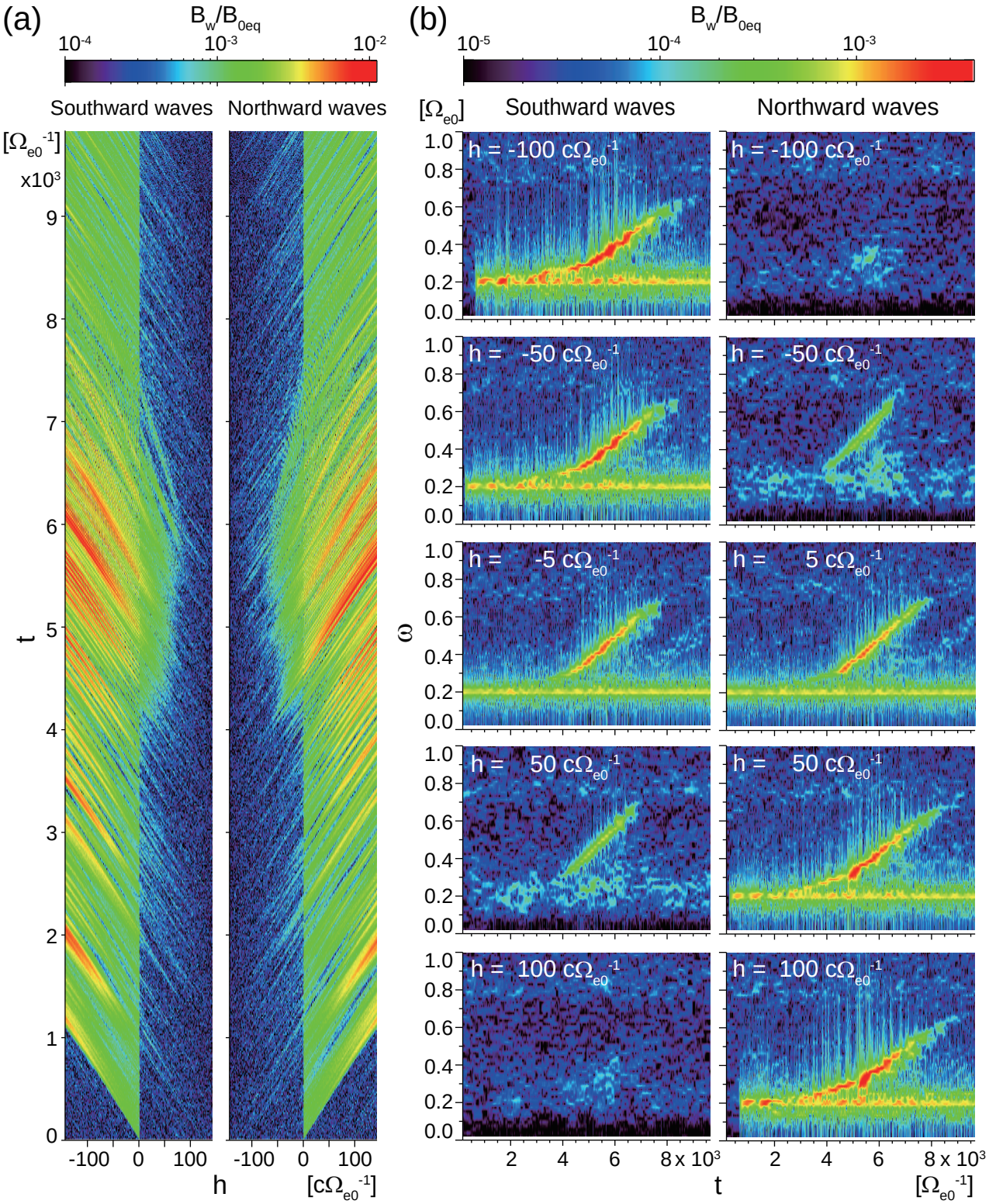

Figure 2. Injection of triggering waves. (a) Temporal evolution of southward and northward propagating waves. Triggering waves are injected at the equator ($h = 0 c\Omega_{e0}^{-1}$) into both hemispheres. Triggered waves created by the triggering waves are excited around the equator. (b) Frequency-time power spectrograms for southward and northward waves at different positions along field line.

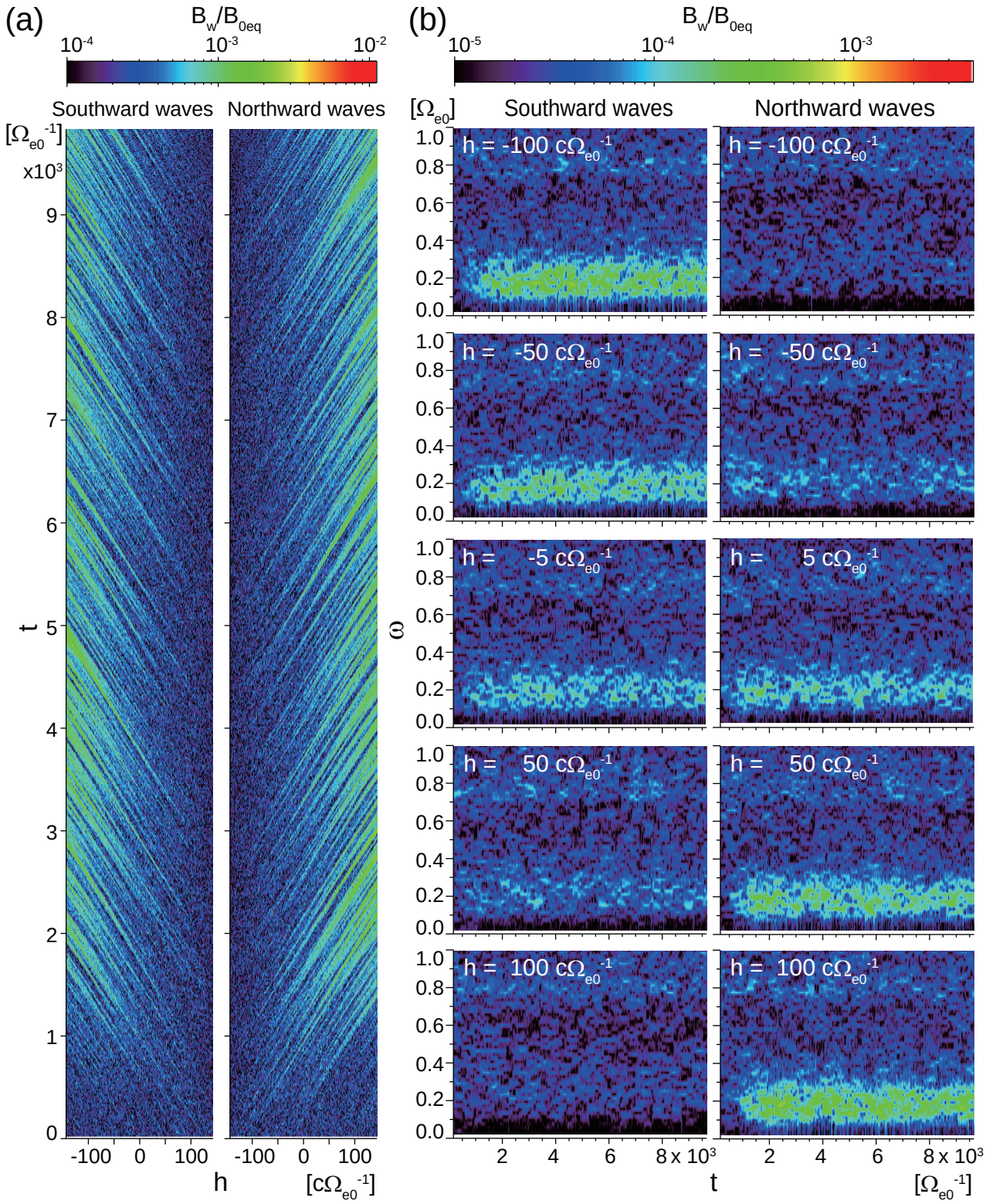

Figure 3. No injection of triggering waves. (a) Temporal evolution of propagating waves which are separated into southward and northward waves. (b) Frequency-time power spectrograms for northward and southward propagating waves.

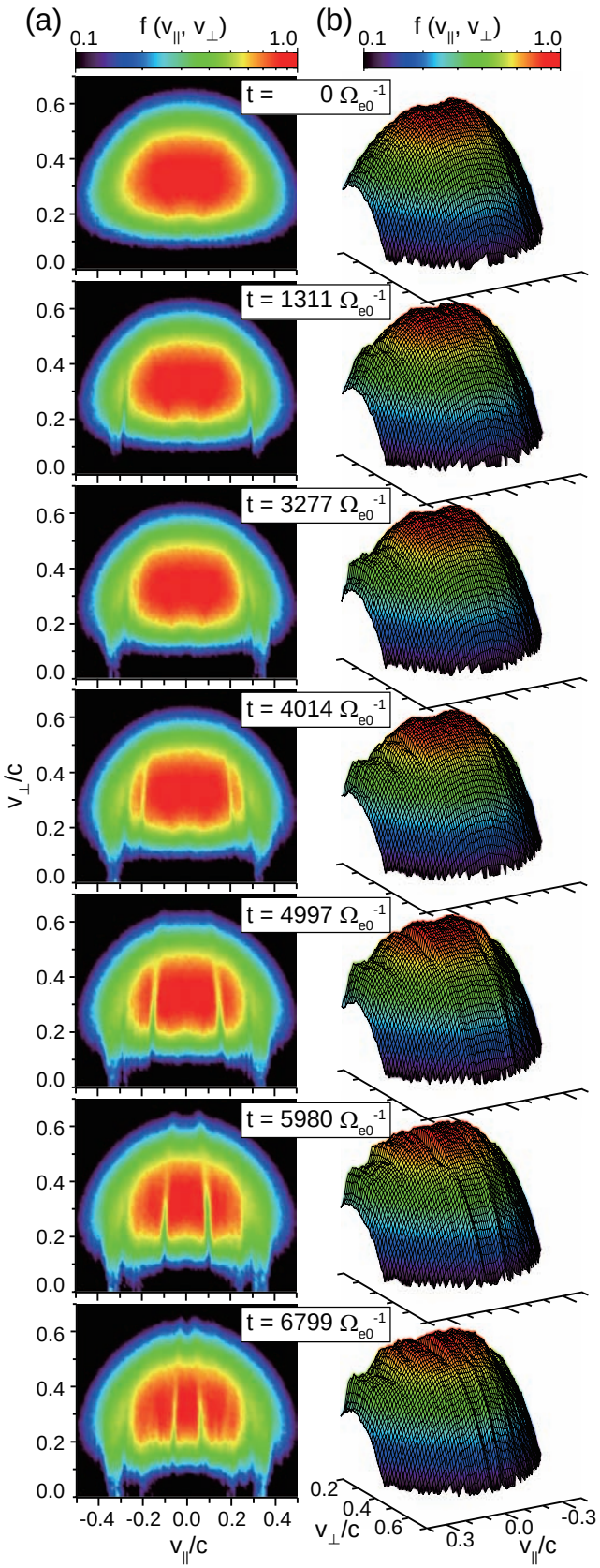

Figure 4. Time evolution of the electron velocity distribution function $f(v_\parallel, v_\perp)$ at the equator. (a) $f(v_\parallel, v_\perp)$ plotted by color contours on a logarithmic scale. (b) Perspective view of the distribution from a high pitch angle.

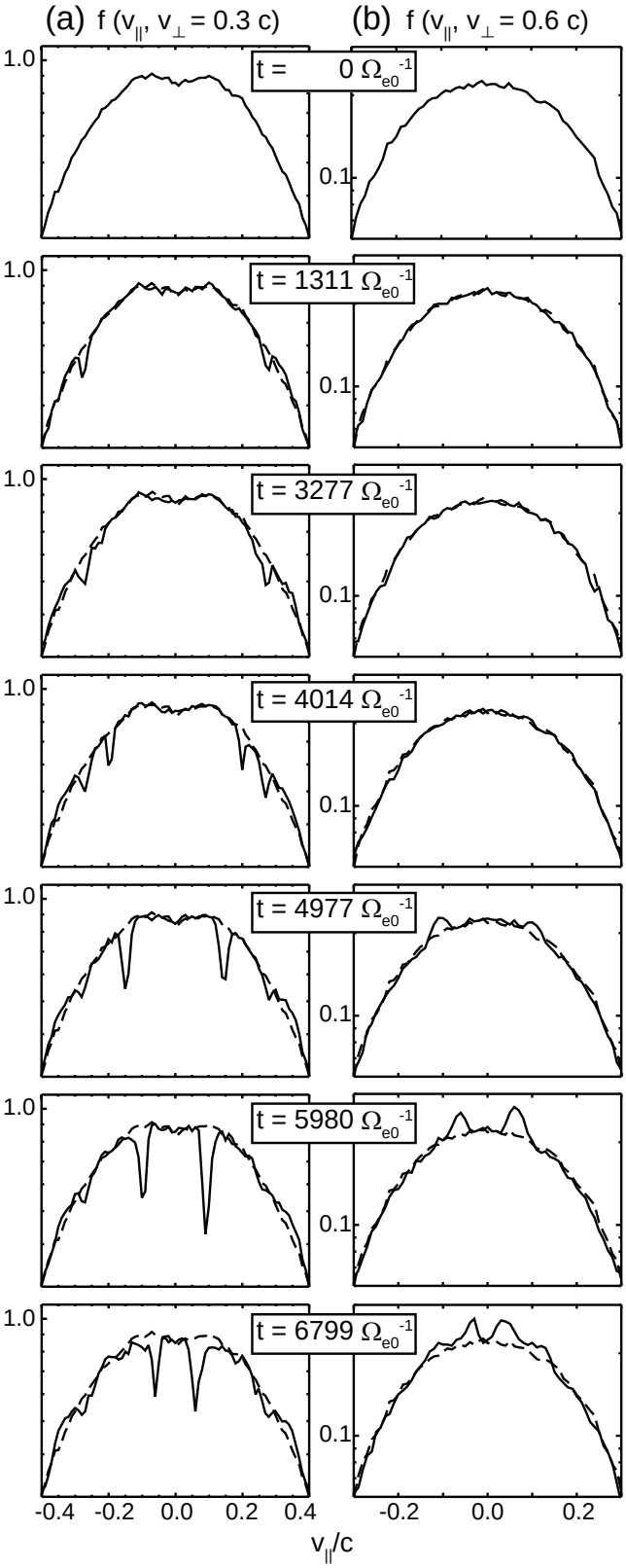

Figure 5. Time evolution of the electron velocity distribution function (a) $f(v_\parallel, v_\perp = 0.3\,c)$ and (b) $f(v_\parallel, v_\perp = 0.6\,c)$ at the equator. Dashed curves represent the initial velocity distribution function $f(v_\parallel)$ at $t = 0\,\Omega_{e0}^{-1}$.

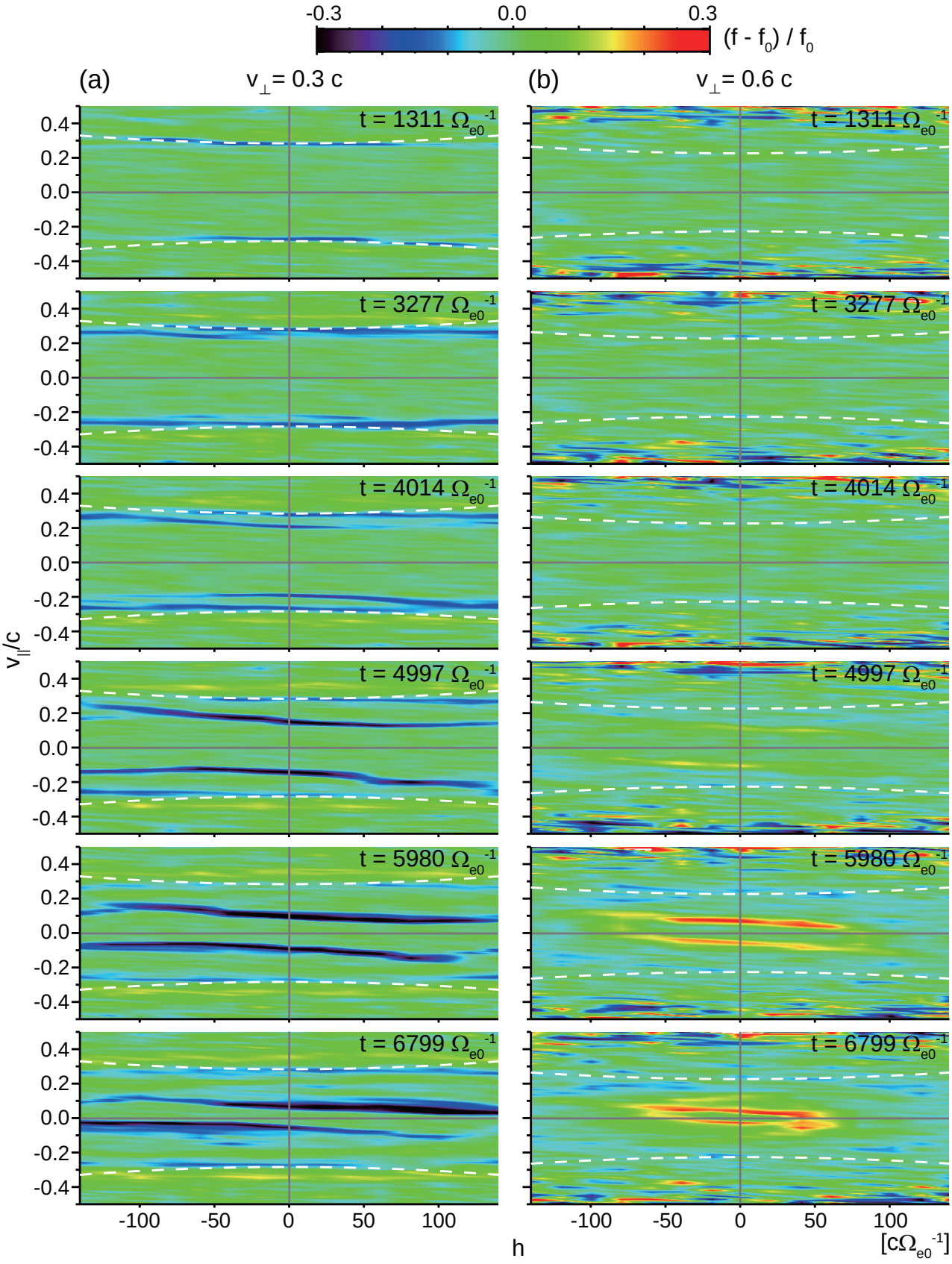

Figure 6. Time evolution of $f(v_\parallel, v_\perp, h)$ at specific perpendicular velocities $v_\perp = 0.3, 0.6c$, from which the initial distribution functions $f_0(v_\parallel, v_\perp, h)$ have been subtracted, and normalized by $f_0(v_\parallel, v_\perp, h)$. White dashed lines represent the resonance velocities for the triggering wave of frequency $\omega = 0.2\,\Omega_{e0}$. Vertical and horizontal gray lines represent the equator ($h = 0\,c\Omega_{e0}^{-1}$) and $v_\parallel = 0\,c$, respectively.

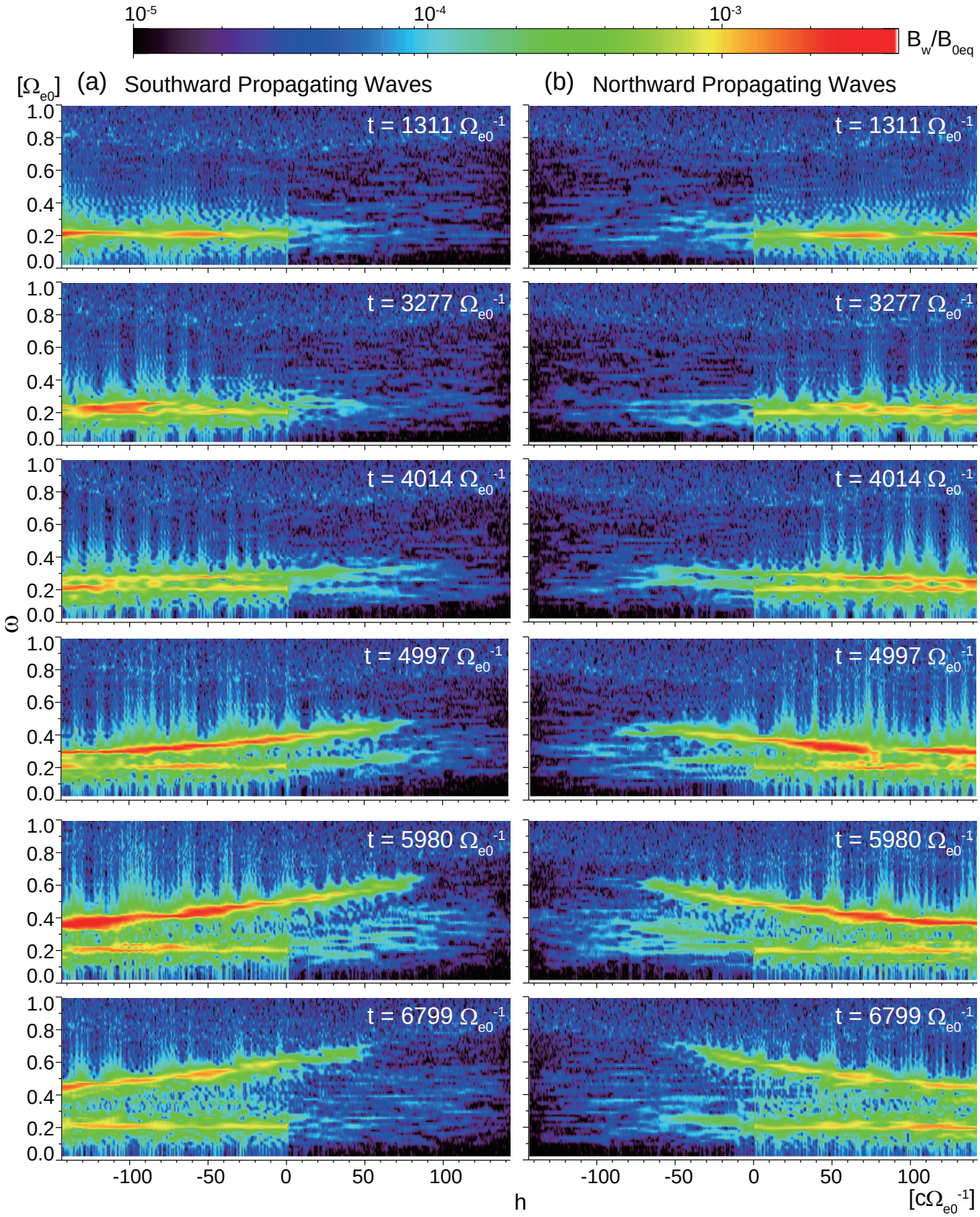

Figure 7. Time evolution of the frequency-spatial power spectrograms of the propagating waves. The waves are separated into southward and northward propagating waves.

Table 1. Simulation parameters

Time step	$0.005\,\Omega_{e0}^{-1}$
Grid spacing	$0.01\,c\Omega_{e0}^{-1}$
Number of grids	32,768
Total number of hot electrons	134,217,728
Total number of cold electrons	16,777,216
Plasma frequency of cold electrons : ω_{pe}	$5\,\Omega_{e0}$
Density ratio of hot electrons to cold electrons : N_h/N_c	6.4×10^{-3}
Thermal momenta of energetic electrons at the equator : $U_{th\parallel}, U_{th\perp}$	$0.24\,c$, $0.31\,c$
Temperature anisotropy : $A = T_\perp/T_\parallel - 1$	0.7
Loss cone parameter : β (equation (1))	0.3
Coefficient of parabolic magnetic field : a	$4.9\times10^{-6}\,(c^{-1}\Omega_{e0})^2$
Frequency of triggering wave (constant)	$0.2\,\Omega_{e0}$
Amplitude of triggering wave (constant) : Ω_w	$1.3\times10^{-3}\,\Omega_{e0}$